Electronic Supplementary Material (ESI) for Materials Horizons.

Supporting Information

High green index electromagnetic interference shields with semiconducting Bi_2S_3 fillers in a PEDOT:PSS matrix

Sanjoy Sur Roy[1], Koushik Ghosh[1], M. Meyyappan[2] and P.K. Giri[1,2,*]

[1]Department of Physics, Indian Institute of Technology Guwahati, Guwahati, 781039 India

[2]Centre for Nanotechnology, Indian Institute of Technology Guwahati, Guwahati, 781039 India

* E-mail: giri@iitg.ac.in

EMI shielding characteristics and relations to scattering parameters

The EMI shielding effectiveness (SE) is the key performance metric, which measures the ability of a material to attenuate the incident EM radiation, given by:

$$SE = 10 \log (P_t/P_i) = 20 \log (|E_t| / |E_i|) = 20 \log (|H_t| / |H_i|) \quad \text{(S1)}$$

where P, E and H denote power, and electric and magnetic field intensities, respectively. The subscripts t and i represent transmitted and incident waves respectively. Three mechanisms contribute to EMI shielding: reflection, absorption and multiple-reflection. The SE of a shielding material is the sum of the contributions due to reflection (SE_R), absorption (SE_A) and multiple reflections (SE_M), all of which are stated in the units of dB.

$$SE = SE_R + SE_A + SE_M \quad \text{(S2)}$$

The contribution from multiple refection is generally assumed to be negligible when the absorption contribution to EMI SE is more than 10 dB or when the shield material is thicker than the skin depth.

The two-port vector network analyzer (VNA) returns four scattering parameters S_{11} (forward reflection coefficient), S_{12} (forward transmission coefficient), S_{21} (reverse transmission coefficient) and S_{22} (reverse reflection coefficient) and they are used to calculate the three key attributes of reflectance (R), transmittance (T) and absorbance (A).

$$R = |S_{11}|^2 = |S_{22}|^2 \quad \text{(S3)}$$

$$T = |S_{12}|^2 = |S_{21}|^2 \quad \text{(S4)}$$

$$A = 1 - R - T \quad \text{(S5)}$$

The reflection (SE_R) and absorption (SE_A) components of the SE are given by:

$$SE_R = 10 \log (1\text{-}R)^{-1} \quad \text{(S6)}$$

$$SE_A = 10 \log (1\text{-}R)/T \quad \text{(S7)}$$

Then the total SE according to relation (S2) is:

$$SE_T = 10 \log (1/T) = -20\log (S_{21}) \quad \text{(S8)}$$

The shielding efficiency (%) is given by 100 x (1-T) which includes all the EM waves that have been reflected and absorbed. Since T is correlated to the measured SE according to equation (S8), SE can be converted to efficiency as follows:

$$\text{Shielding efficiency (\%)} = 100 \times (1 - 10^{-(SE/10)}) \quad \text{(S9)}$$

For example, SE values of 20, 40, 60, 80 and 100 dB correspond to shielding efficiencies of 99.0, 99.99, 99.9999, 99.999999 and 99.99999999 % respectively.

Green index

Green index (GI) is a measure of the relative importance of the absorption and reflection mechanisms to the total shielding effectiveness. The green index is given by[1, 2]:

$$GI = S_{11}^{-2} - (S_{21}^2/S_{11}^2) - 1 \quad \text{(S10)}$$

Substitution of relations (S3) - (S5) in (S10) yields a simple relation for GI as

$$GI = A/R \quad \text{(S11)}$$

The measured R and A must be used to assess the relative contributions of reflection and absorption to the observed shielding performance, and SE_R and SE_A - two quantities expressed in dB - cannot be used for this purpose as clearly pointed out by Peng and Qin.[3] To illustrate this, let us consider a hypothetical case of a high 60 dB SE performance, which gives T as 1.0×10^{-6} from

eqn. (S8). Total shielding is given by (1-T) = A+R. The total shielding in this hypothetical case is close to 1 since T is very small. If this hypothetical total shielding is arbitrarily split as R = 0.9 and A = 0.1, then absorption contributes only 10% to the total shielding while reflection is responsible for 90% with a green index of just 0.11. The SE_R and SE_A values corresponding to R = 0.9 and A = 0.1, as calculated from eqns. (S6) and (S7), are 10 dB and 50 dB respectively, adding to a total SE of 60 dB as assumed above. Assessing relative contributions of the two mechanisms to the observed SE from these two quantities in dB units leads to an erroneous conclusion of absorption dominance, which is not true. This is because reflection and absorption losses stated in dB do not represent the actual reflected and absorbed power and therefore, cannot determine the relative contributions of reflection and absorption to the total shielding.[3] Additional splits of R and A for this hypothetical case in Table S1 always show higher SE_A than SE_R even when R is high except when R is practically close to unity. This is true for another hypothetical case of a nominal 30 dB that meets the minimum commercialization requirement as seen in Table S2.

Table S1. SE_A and SE_R values for a hypothetical shielding of 60 dB and various splits of R and A.

R	A	GI	SE_R, dB	SE_A, dB	SE_T, dB
0.99999	0.00001	1×10^{-5}	50	10	60
0.99	0.01	0.010	20	40	60
0.9	0.1	0.111	10	50	60
0.8	0.2	0.250	6.99	53.01	60
0.5	0.5	1.0	3.01	56.99	60
0.1	0.9	9.0	0.458	59.542	60

The difference between the two sets of indicators (A and R) vs. (SE_A and SE_R) can be understood when realizing that only a (left-over) portion of the incident EM waves enter the body of the shield after initial reflection on the surface. Then, SE_R represents the ratio of the reflected energy to the energy of the incident EM waves whereas SE_A denotes the ratio of the absorbed

energy to the energy of the EM waves that enter the body of the shield and not the original incident waves. Hence, the denominators are clearly different in the cases of SE_A and SE_R.[4]

Table S2. SE_A and SE_R values for a hypothetical shielding of 30 dB and various splits of R and A.

R	A	GI	SE_R, dB	SE_A, dB	SE_T, dB
0.99	0.009	9.1×10^{-3}	20	10	30
0.9	0.099	0.11	10	20	30
0.8	0.199	0.211	6.99	23.01	30
0.5	0.499	0.998	3.01	26.99	30
0.1	0.899	8.99	0.458	29.542	30

Dielectric constant of the shield

According to Debye theory, the correlation between real component of dielectric constant (ε′) and imaginary component of dielectric constant (ε′′) is given by the relation:[1]

$$\left(\varepsilon' - \frac{\varepsilon_S + \varepsilon_\infty}{2}\right)^2 + (\varepsilon'')^2 = \left(\frac{\varepsilon_S - \varepsilon_\infty}{2}\right)^2 \qquad \text{(S12)}$$

Where, the static electrical permittivity and the dielectric permittivity at large frequency limit are denoted as ε_s and ε_∞, respectively.

The complex permittivity of the prepared shields were determined from the measured S-parameters by employing the Nicolson−Ross−Weir (NRW) method.[5] This method is incorporated in most VNA software and correlates reflection (S_{11}) and transmission (S_{21}) coefficients to permittivity and permeability through the relations of the latter two with attenuation and loss tangent.

Characterization techniques

The morphology of the prepared films was studied by field emission scanning electron microscopy (FESEM) (Sigma, Zeiss, Germany) and transmission electron microscopy (TEM) (JEM-2100F; JEOL, Japan), including a high-resolution TEM (HRTEM) operating at 200 kV. The elemental composition and elemental mapping of pure Bi_2S_3 and nanocomposite films were obtained by energy dispersive X-ray analysis (EDS) (Sigma, Zeiss, Germany). The crystallinity of the films was examined by X-ray diffractometer (SmartLab 9kw, Rigaku, Japan) with wavelength λ=1.5406 Å of Cu-Kα radiation at a scan rate 5°min^{-1}. Raman spectra were collected using a micro-Raman spectrometer (HORIBA, LabRam HR) and He-Ne laser (excitation wavelength λ_{ex} = 532 nm). Surface compositional analysis was performed by X-ray photoelectron spectroscopy (XPS) (PHI5000VERSAPROBE III, ULVAC-PHI Inc., Japan). The XPSPEAK 4.1 software was used to analyze the XPS spectra.

The electrical conductivity of the films was measured by a standard four-probe technique using Keithly 2400 Source meter. Commercially available silver ink was deposited onto the surface of the composite film and the four probes were then placed on it. All the measurements were done at ambient pressure and room temperature. The EM parameters were measured using a vector network analyzer (VNA, Keysight, N5232A) over the X-band (8.2-12.4 GHz) and Ku-band (12.4-18 GHz) with films cut into rectangular shapes (22.9 × 10.2 mm for X- band and 15.8×7.9 mm for Ku-band). The standard two-port Solt calibration (short, open, load, thru) was performed prior to S-parameter measurement.

Computational details

Density Functional Theory (DFT) calculations were performed using the Quantum Espresso software package.[6] The exchange-correlation interaction was addressed using the Perdew-Burke-Ernzerhof (PBE) functional, with Generalized Gradient Approximation (GGA).[7] Additionally, the Grimme-D3 method was employed throughout the computations to consider van der Waals corrections.[8] A plane wave cut-off energy of 60 Ry was chosen for these calculations, accompanied by a Monkhorst pack k-point grid of 12 × 12 × 1 to sample the Brillouin zone.[9] A vacuum layer of 15 Å was employed in the z-direction to avoid the periodic interaction. The atomic electronic configuration was modeled using Vanderbilt ultra-soft pseudopotentials in reciprocal space. The energy convergence threshold was set to 1×10^{-4} Ry to ensure accuracy. The analysis involved the examination of the charge density distribution. The charge density distribution was visualized by

utilizing VESTA software.[10] Additionally, the charge density difference (CDD), denoted as ρ_{cdd}, was computed using the following relation:

$$\rho_{cdd} = \rho_{BSPP} - \rho_{BS} - \rho_{PP}$$

Where, ρ_{BSPP}, ρ_{BS} and ρ_{PP} represent the charge density of BSPP nanocomposite, BS and PP, respectively.

Shielding effectiveness of a thin aluminum foil

The shielding effectiveness of a common kitchen aluminum foil used in food wrapping (thickness of about 20 μm) was measured here for reference and found to be 99.5 dB averaged over the X-band (Fig. S1). The corresponding average reflectance (R) and absorbance (A) values are 0.95 and 0.05, giving a green index of merely 0.053.

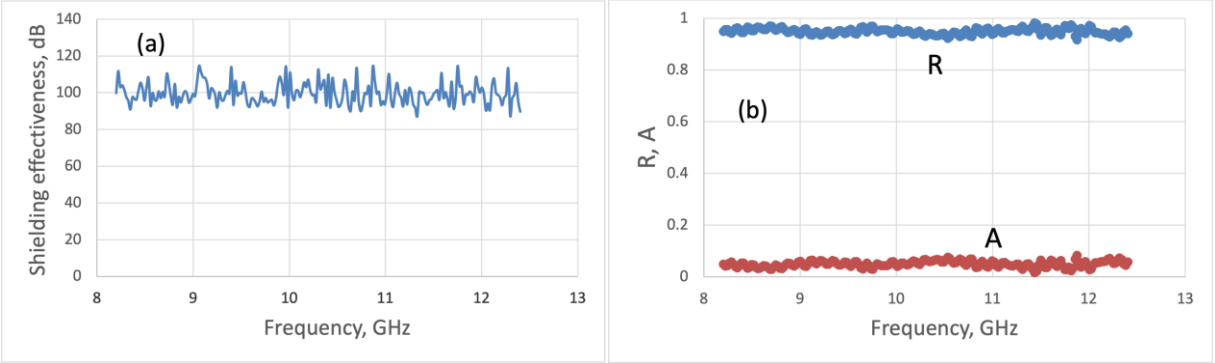

Fig. S1 Shielding effectiveness (left) and values of reflectance and absorbance (right) of an aluminum foil.

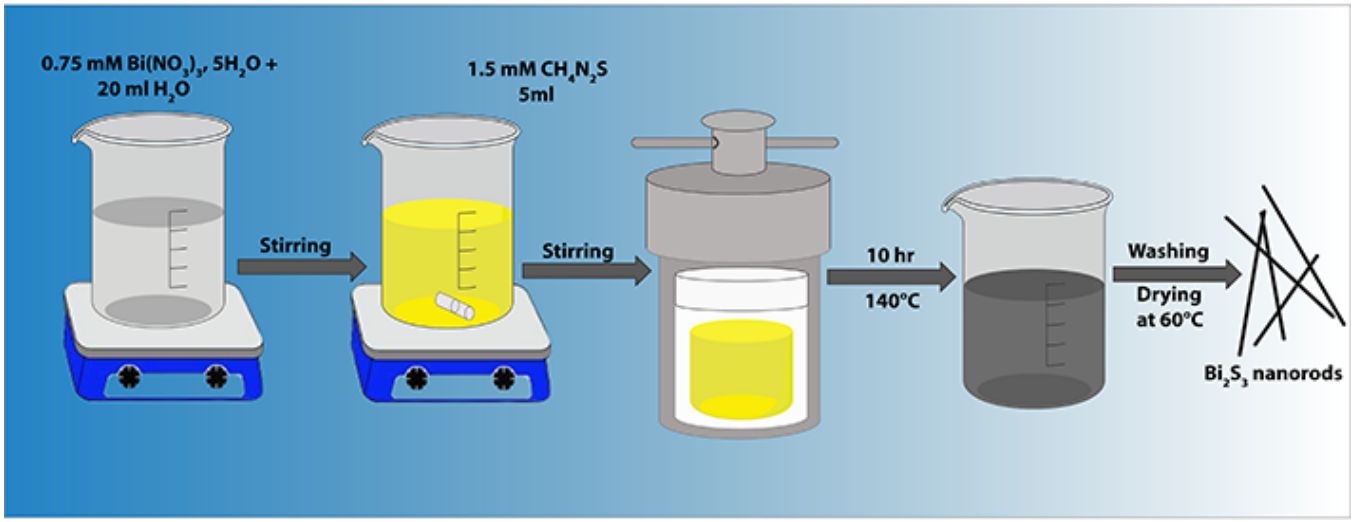

Fig. S2 Schematic of one-step hydrothermal synthesis of Bi_2S_3 nanorod.

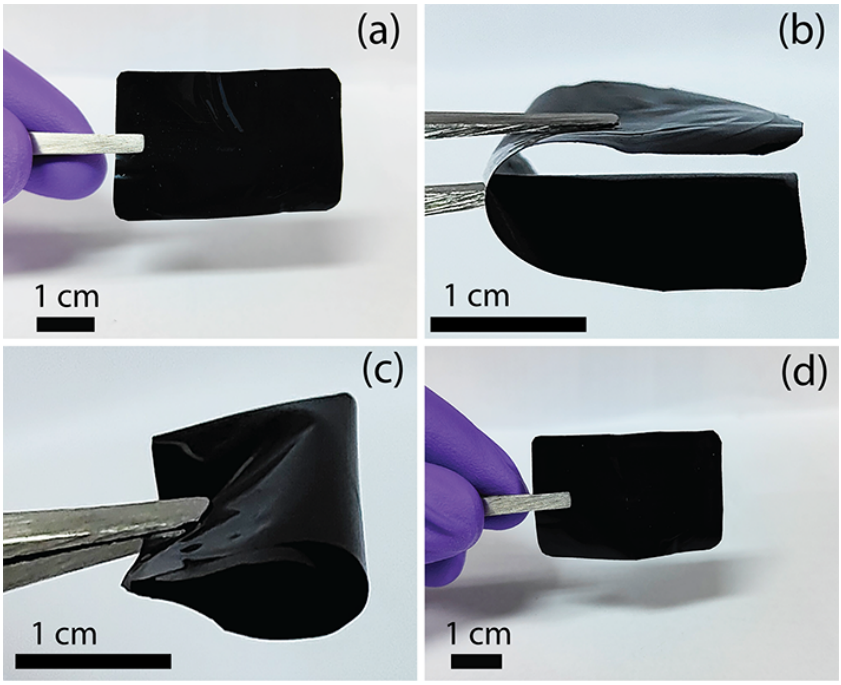

Fig. S3 Optical image of an as-prepared BSPP film (a) before folding, (b) one time folded, (c) multiple folded and (d) after unfolding back to initial position, illustrating its foldable and flexible characteristics. The thickness of the as-prepared BSPP film is ~44 µm.

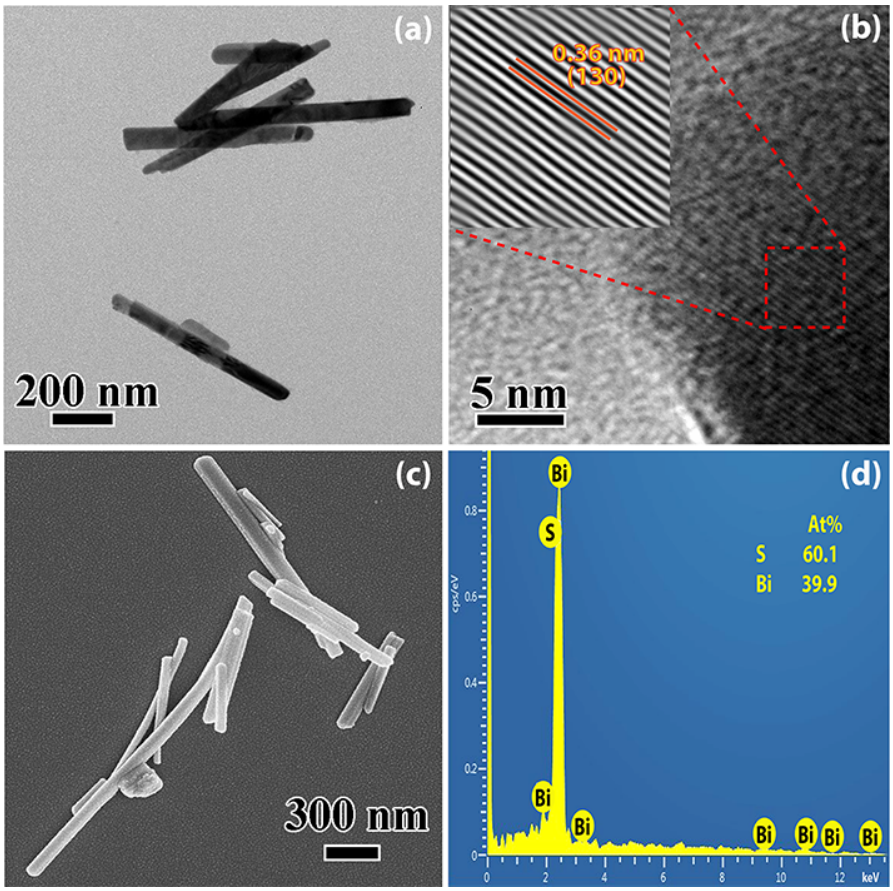

Fig. S4 (a) TEM, (b) HRTEM and (c) FESEM images of Bi_2S_3 nanorods. (d) EDS data of Bi_2S_3 nanorods.

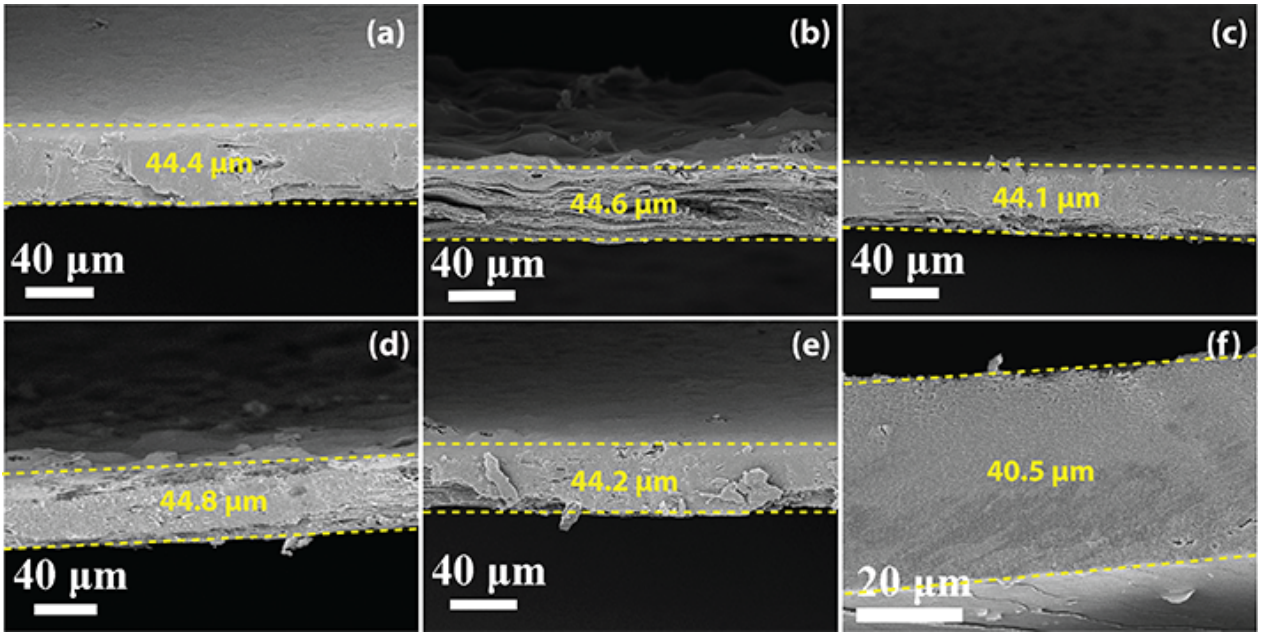

Fig. S5 Thicknesses of the nanocomposite films measured from the cross-sectional FESEM image of (a) BSPP-5, (b) BSPP-7.5, (c) BSPP-10, (d) BSPP-12.5, (e) BSPP-15 and (f) PP films.

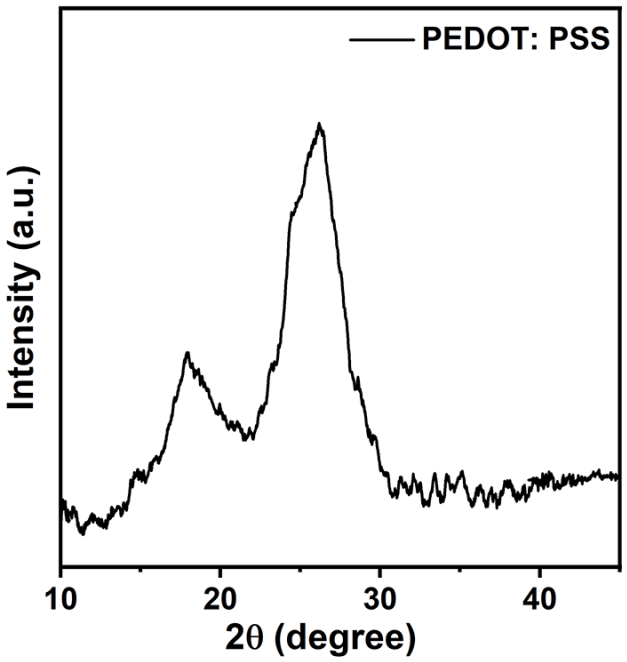

Fig. S6 XRD pattern of pristine PEDOT:PSS polymer (PP) film.

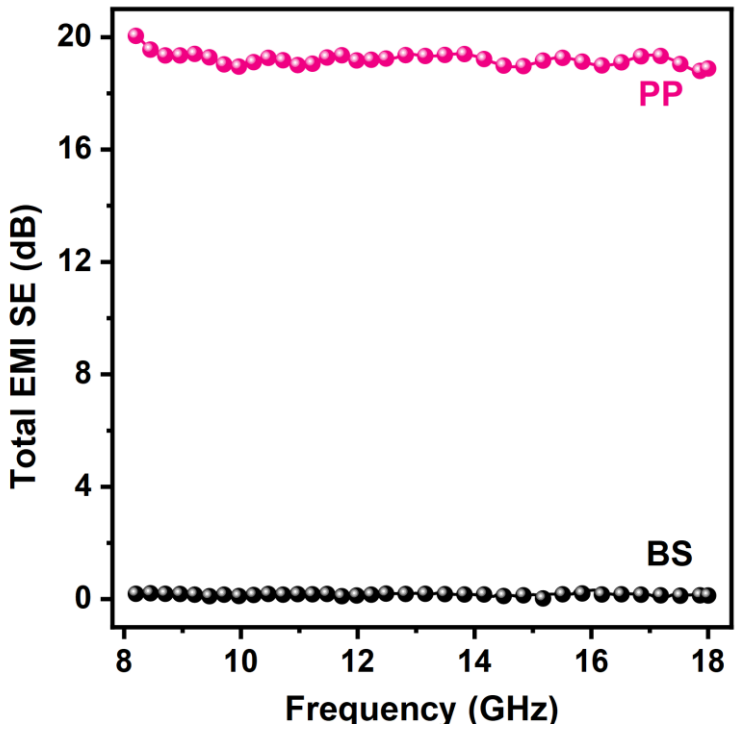

Fig. S7 The shielding effectiveness (SE) value of the two constituent materials, Bi_2S_3 (BS) and PEDOT:PSS (PP).

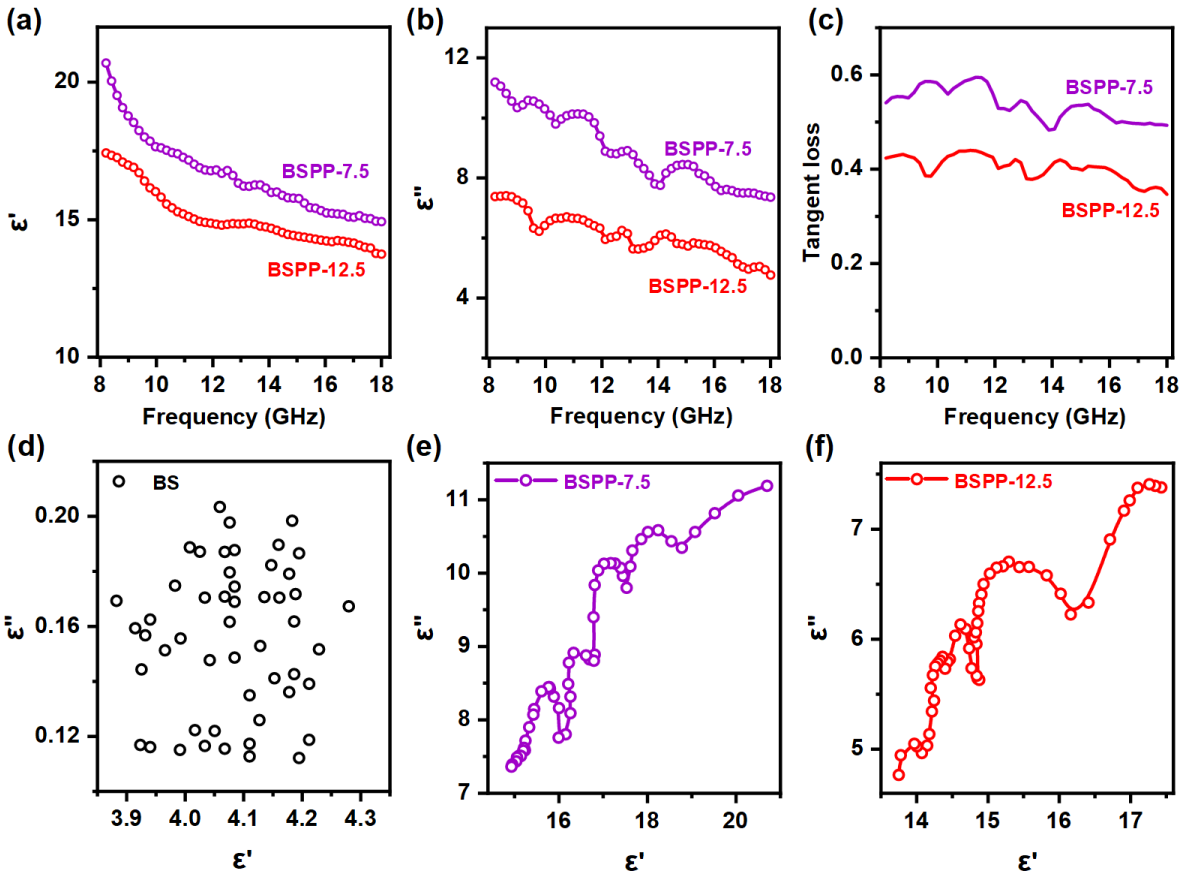

Fig. S8 Dielectric permittivity of the as-prepared BSPP-7.5 and BSPP-12.5 films (a) Real (ε′) and (b) Imaginary (ε′′) component of the dielectric constant. (c) Tangent loss as a function of frequency. Cole-Cole plot of (d) BS, (e) BSPP-7.5 and (f) BSPP-12.5, respectively.

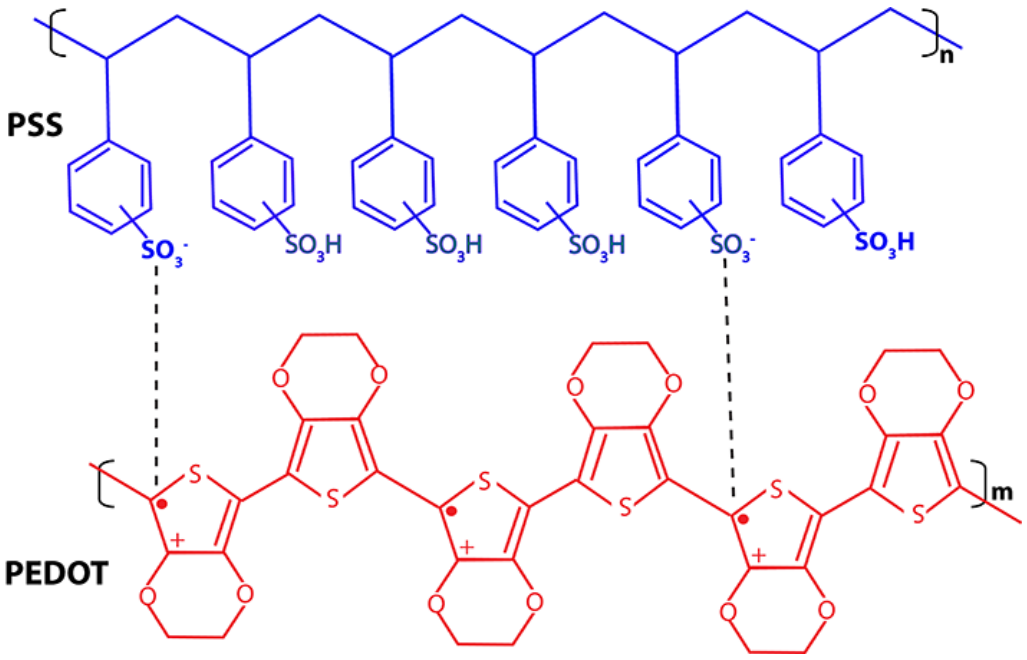

Fig. S9 Chemical structure of the PEDOT:PSS polymer.

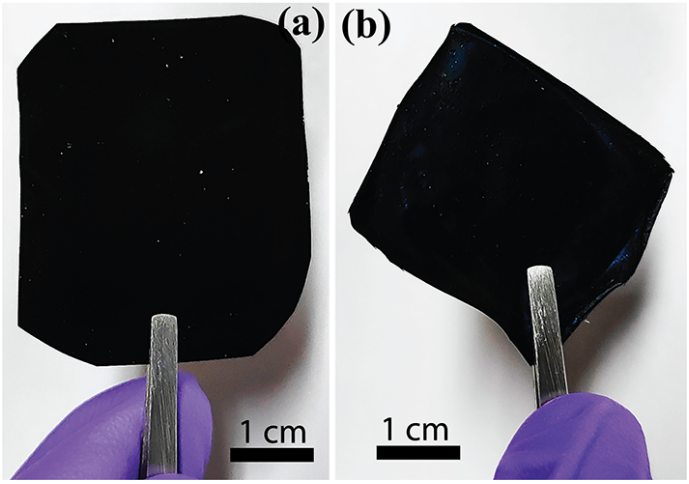

Fig. S10 Optical image of the BSPP film (a) before and (b) after H_2SO_4 treatment. The thickness of the BSPP film after H_2SO_4 treatment is ~ 35 µm.

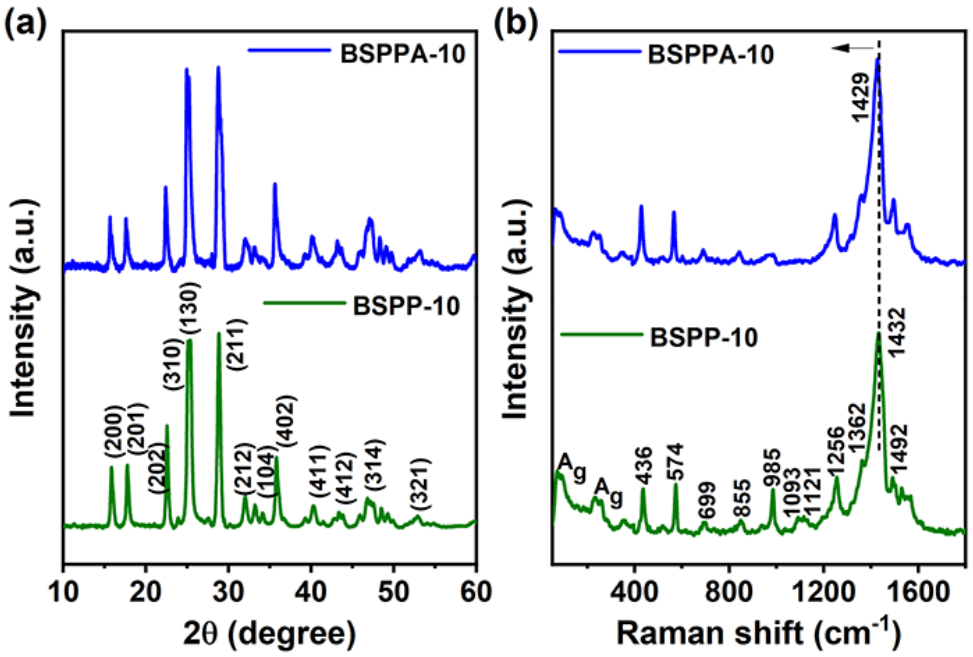

Fig. S11 (a) XRD pattern of the BSPP-10 film after acid-treatment (BSPPA-10). (b) Raman spectra of the BSPP-10 film after acid-treatment (BSPPA-10).

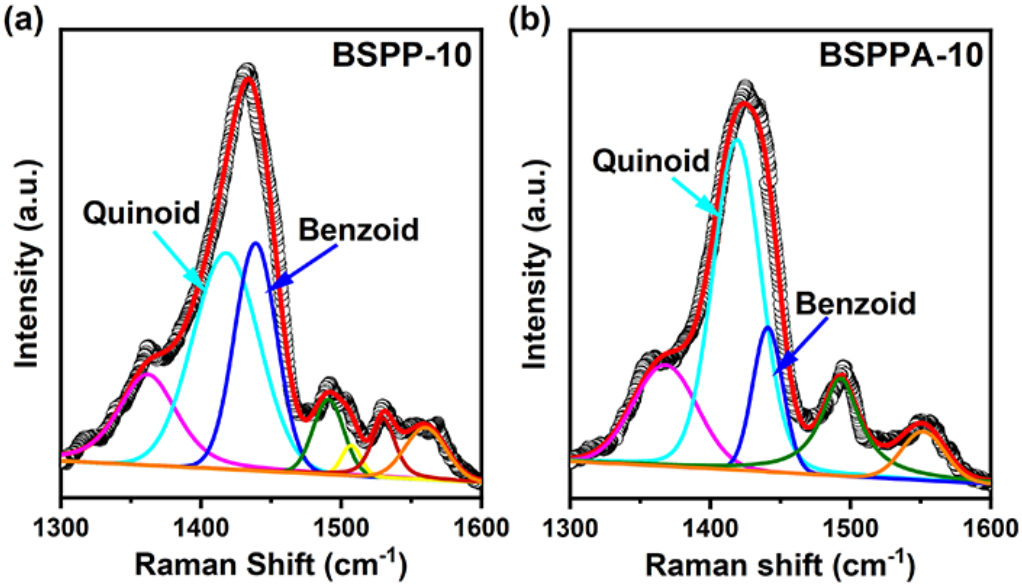

Fig. S12 Deconvolution of Cα=Cβ symmetric stretching vibration peak of (a) BSPP-10 and (b) BSPPA-10 films, respectively.

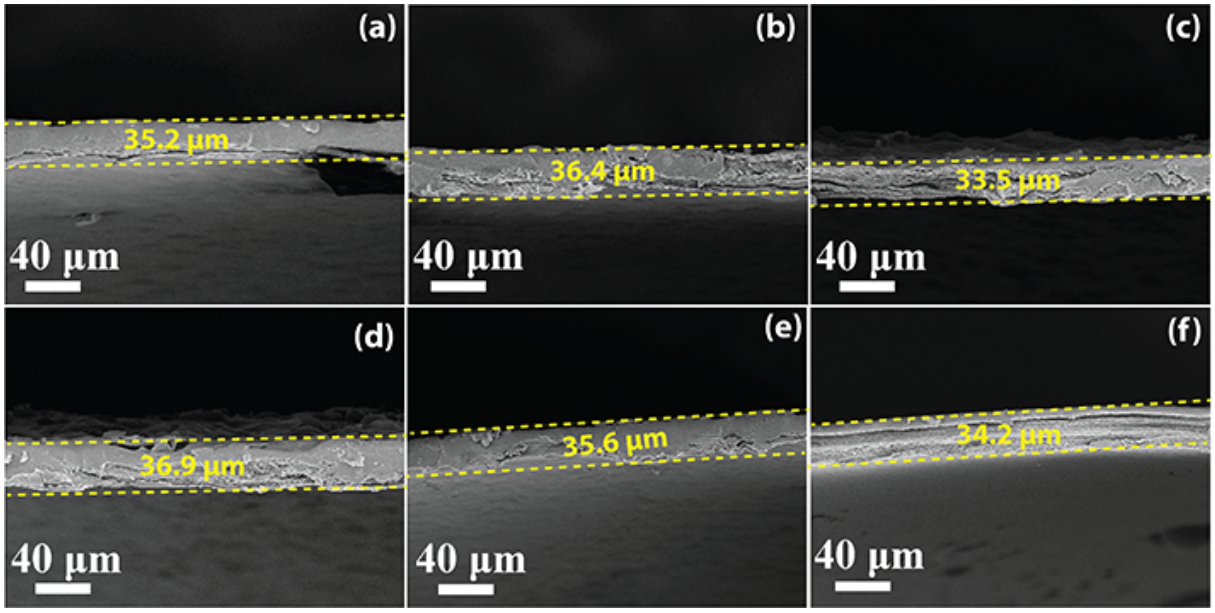

Fig. S13 Thicknesses of the acid-treated nanocomposite films measured from the cross-sectional FESEM image of (a) BSPPA-5, (b) BSPPA-7.5, (c) BSPPA-10, (d) BSPPA-12.5, (e) BSPPA-15 and (f) PPA films.

References

1. S. S. Roy, K. Ghosh, M. Meyyappan and P. Giri, *ACS Appl. Nano Mater.*, 2023, **6**, 23357-23369.
2. D.-Q. Zhang, T.-T. Liu, J.-C. Shu, S. Liang, X.-X. Wang, J.-Y. Cheng, H. Wang and M.-S. Cao, *ACS Appl. Mater. Interfaces*, 2019, **11**, 26807-26816.
3. M. Peng and F. Qin, *J. Appl. Phys.*, 2021, **130,** 225108.
4. J. Cheng, C. Li, Y. Xiong, H. Zhang, H. Raza, S. Ullah, J. Wu, G. Zheng, Q. Cao and D. Zhang, *Nano-Micro Lett.*, 2022, **14**, 80.
5. W. B. Weir, *Proc. IEEE*, 1974, **62**, 33-36.
6. P. Giannozzi, S. Baroni, N. Bonini, M. Calandra, R. Car, C. Cavazzoni, D. Ceresoli, G. L. Chiarotti, M. Cococcioni and I. Dabo, *J. Phys.: Condens. Matter*, 2009, **21**, 395502.
7. J. P. Perdew, K. Burke and M. Ernzerhof, *Phys. Rev. Lett.*, 1996, **77**, 3865.
8. J. Moellmann and S. Grimme, *J. Phys. Chem. C*, 2014, **118**, 7615-7621.
9. H. J. Monkhorst and J. D. Pack, *Phys. Rev. B*, 1976, **13**, 5188.
10. K. Momma and F. Izumi, *J. Appl. Crystallogr*, 2008, **41**, 653-658.